PROPOSED DYNAMIC SOIL PRESSURE DIAGRAM ON RIGID WALLS

M. Moayyedian, K. Moslem* and A. Shooshtari

Department of Civil Engineering, Ferdowsi University of Mashhad
P.O. Box 91775-1111, Mashhad, Iran
moayyedian@yahoo.com - kmoslem@yahoo.com - ahmadshooshtari@yahoo.com

*Corresponding Author

(Received: December 9, 2006 – Accepted in Revised Form: May 9, 2008)

Abstract Using finite element nonlinear analysis, the dynamic soil pressure on perimeter retaining walls of structures is investigated. Nonlinear Drucker Prager failure criterion is used to model the soil behavior in the near field. The far field soil and the middle structure are assumed to behave as linear elastic materials. The soil-wall interface behavior is modeled incorporating nonlinear interface elements. The internal friction angle of the soil is found to be an important factor in the dynamic lateral pressure that has been neglected in the previous investigations. Furthermore, a new diagram is proposed to determine lateral seismic soil thrust on rigid walls.

Keywords Retaining Walls, Rigid Walls, Dynamic Pressure, Soil Structure Interaction

چکیده با به کار بردن تحلیل غیرخطی اجزای محدود، فشار دینامیکی خاک روی دیوارهای محیطی سازه ها بررسی شده است. معیار دراکر پراگر برای الگوسازی رفتار خاک در ناحیه نزدیک مورد استفاده واقع شده است. فرض گردیده است که خاک ناحیه دور و سازه دارای رفتار خطی باشند. برای الگوسازی سطح مشترک خاک – دیوار اجزای واسط غیر خطی به کار رفته است. مشاهده گردید که زاویه اصطکاک داخلی خاک عامل مهمی در تعیین فشار جانبی دینامیکی خاک است که در پژوهش های پیشین مورد توجه قرار نگرفته است. افزون بر این یک نمودار جدید برای تعیین فشار لرزه ای خاک پیشنهاد گردیده است.

1. INTRODUCTION

Much studies have been carried out on the dynamic response of cantilever retaining walls but the embedded perimeter walls of structures have received relatively less attention. Though the dynamic behavior of these two types of retaining walls is different, the dynamic soil pressure relations of cantilever walls, such as Mononobe Okabe, are sometimes erroneously used for perimeter walls.

For the first time Wood, et al [1] developed an equivalent static elastic solution for the dynamic soil pressure on non-yielding walls, using linear elastic finite element method [1]. In his analysis a uniform soil layer is assumed to act on the wall and the soil-wall system is resting on a rigid base. The exciting motion is a harmonic wave. The pressure and its center is a function of Poisson's ratio of the soil medium. If the pressure is assumed to change linearly through the height of the wall, the pressure diagram for a Poisson's ratio of the soil equal to 0.2 is similar to that shown in Figure 1. In this diagram, and other forthcoming diagrams, p_D is the dynamic soil pressure, z is the height coordinate from the base of the wall and H is the height of the wall. A is the maximum ground acceleration with respect to gravity acceleration and γ is the density of the soil.

Wu, et al [2] used an approximate method based on a modified shear beam model and also a finite element nonlinear elastic analysis to develop charts for seismic thrust against rigid walls [2]. In their model the shear modulus of the soil is a function of the depth. Three types of constant, linear and parabolic varying shear modulus are considered. The design charts are functions of the fundamental frequency of the soil-wall system and the ratio of this frequency to the base acceleration frequency. They concluded

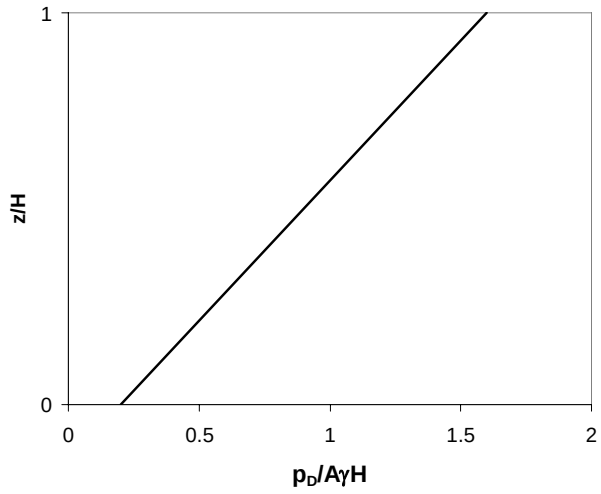

Figure 1. Wood diagram for dynamic soil pressure.

that Wood's diagram underestimates seismic soil pressure when the period of the soil-wall system approaches the period of the earthquake motion. They found that the total lateral thrust on the wall can be up to about 40 percent higher than Wood solution.

A damping ratio equal to 10 percent was used in the Wu and Finn charts. They have also studied the effect of soil damping ratio on the soil thrust and found that if the soil damping ratio is reduced to 5 percent of the critical damping, the total soil pressure can be increased up to 15 percent. Also, they found that by increasing the poisson's ratio of the soil, the dynamic pressure of the soil will be increased. As an example, if the soil poisson's ratio is increased from 0.3 to 0.5, the total thrust will be multiplied by 1.18.

Ostadan, et al [3] employed a simple finite element model to study the dynamic behavior of perimeter retaining walls under seismic loading using SASSI software [3]. The soil medium was modeled by elastic plane elements and no interface elements were used. It was found that the maximum amplification takes place at an input frequency corresponding to the soil column natural frequency. The dynamic pressure distribution is given by a fifth order polynomial.

Younan, et al [4] have analyzed the response of a retaining wall clamped at the bottom edge and hinged at the top [4]. Such boundary conditions can be a simple model for a perimeter wall. The soil was modeled by a series of elastically supported semi-infinite horizontal bars with distributed mass and damping. The far field was also modeled as a shear beam. For harmonic and transient base accelerations, different response modification factors are applied to a base pressure diagram.

The ASCE standard for nuclear structures uses Wood's pressure diagram to estimate dynamic pressure on embedded perimeter retaining walls [5]. The Greek Regulatory Guide E39/93 (GRG) proposes the dynamic lateral soil pressure diagram shown in Figure 2 to be used for bridge abutments with top displacements less than 0.05 percent of the height of the wall [6]. Though GRG diagram gives 10 percent higher lateral force in comparison to ASCE standard, the center of pressure in GRG diagram is 0.05H lower than that, recommended by ASCE.

In all the above mentioned studies the soil has been assumed to behave as a linear material and no attention has been given to the interface behavior. Also, the effect of soil internal friction angle, has been neglected. These effects will be considered in this paper.

2. BASIS OF THE MODEL

In this research, finite element method has been

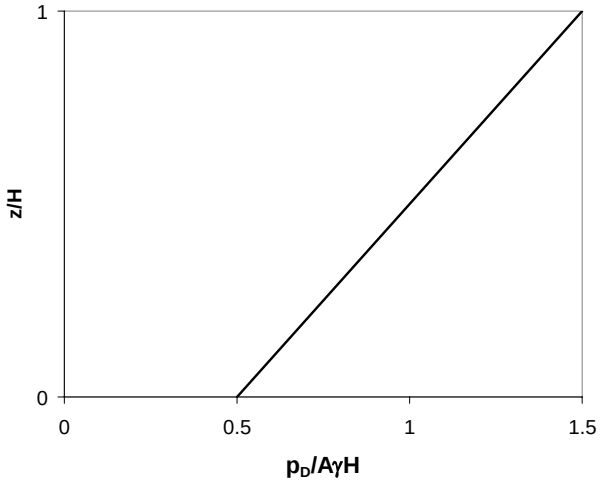

Figure 2. GRG seismic soil pressure diagram.

used to model structure-wall-soil system. The model, shown in Figure 3, consists of plane strain linear elements for the structure, the wall and the far field soil and nonlinear plane strain elements for the near field soil and the interface between soil and the wall. Damping elements are used at vertical boundaries and the base acceleration is applied to the horizontal base boundary.

The distance between the vertical boundaries and the walls has been chosen by a sensitivity analysis, such that the soil pressure on the walls does not change more than 2 percent by increasing the distance. Also, at a distance from the walls soil does not reach the yield stress. This distance was found to be about 30 meters in this study by inspecting the stress levels in the soil medium.

The stress and strain vectors are defined as:

$$\{\sigma\} = \begin{bmatrix} \sigma_x \\ \sigma_y \\ \tau_{xy} \end{bmatrix} \quad (1)$$

$$\{\varepsilon\} = \begin{bmatrix} \varepsilon_x \\ \varepsilon_y \\ \gamma_{xy} \end{bmatrix} \quad (2)$$

The elastic constitutive matrix assuming plane strain behavior can be written as:

$$\left[C^E\right] = \begin{bmatrix} C^{E1} & C^{E2} & 0 \\ C^{E2} & C^{E1} & 0 \\ 0 & 0 & C^{E3} \end{bmatrix} \quad (3)$$

$$C^{E1} = E(1-\nu)/[(1+\nu)(1-2\nu)] \quad (4)$$

$$C^{E2} = E\nu/[(1+\nu)(1-2\nu)] \quad (5)$$

$$C^{E3} = G \quad (6)$$

E, G and ν are the modulus of elasticity, shear modulus and poisson's ratio of the soil, respectively. The finite element formulation of the wall, middle structure and the far field soil can be achieved using this elastic constitutive matrix.

The near field soil behavior is assumed to be isotropic linear elastic perfectly plastic. The nonlinear behavior of the soil is modeled using perfectly plastic Drucker Prager failure criteria [7]:

$$F = \alpha I_1 + \sqrt{J_2} \quad (7)$$

In this equation, I_1 and J_2 are the first stress invariant and second deviatory stress invariant, respectively. α is found as:

$$\alpha = \frac{2\sin\varphi}{\sqrt{3}(3-\sin\varphi)} \quad (8)$$

where φ is the internal friction angle of the soil. Also, tension cutoff is used to prevent tensile stresses occur in the soil medium.

Using this yield function, the elastoplastic constitutive matrix can be found as [8]:

$$\left[C^{EP}\right] = \begin{bmatrix} C^{EP1} & C^{EP2} & C^{EP3} \\ C^{Ep2} & C^{Ep4} & C^{EP5} \\ C^{EP3} & C^{EP5} & C^{Ep6} \end{bmatrix} \quad (9)$$

$$C^{EP1} = C^{E1}(\beta_1 s_{11} + \beta_2)^2 \quad (10)$$

$$C^{EP2} = C^{E2}(\beta_1 s_{11} + \beta_2)(\beta_1 s_{22} + \beta_2) \quad (11)$$

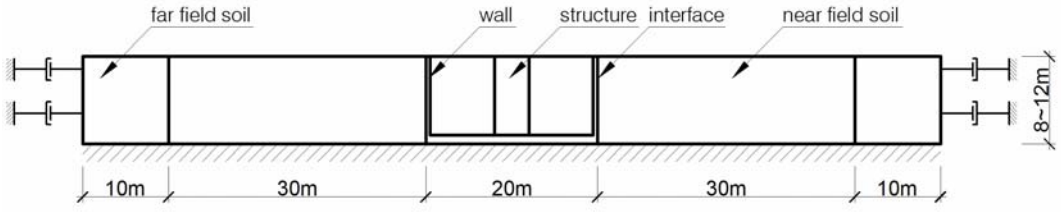

Figure 3. Analysis model.

$$C^{EP3} = (\beta_1 s_{11}+\beta_2) (\beta_1 s_{12}) \quad (12)$$

$$C^{EP4} = C^{E1}(\beta_1 s_{22}+ \beta_2)^2 \quad (13)$$

$$C^{EP5} = (\beta_1 s_{22}+ \beta_2) (\beta_1 s_{12}) \quad (14)$$

$$C^{EP6} = C^{E3}(\beta_1 s_{12})^2 \quad (15)$$

$$\beta_1 = E/[2\sqrt{J_2}(1+\nu)\sqrt{A}] \quad (16)$$

$$\beta_2 = E\alpha/[(1-2\nu)\sqrt{A}] \quad (17)$$

$$A = [E(1-2\nu)+6E(1+\nu)\alpha 2]/[2(1+\nu)(1-2\nu)] \quad (18)$$

In these equations, s_{ij} is the deviatory stress.

The near field soil finite element formulation is based on the elastic and elastoplastic constitutive matrices presented in Equations 3 and 9.

It has been recommended that the same nonlinear normal constitutive law be used for the soil medium and the interface elements [9,10]. Thus Drucker Prager failure envelope is also used to model the continuum interface element normal behavior.

In the stick mode the interface behavior is assumed to be linear elastic. If the material yields, slip occurs between the wall and the soil. In this state, the shear stiffness and shear stresses are set equal to zero. Thus, the elastoplastic constitutive matrix can be written as:

$$\left[C^{EP}\right] = \begin{bmatrix} C^{EP1} & C^{EP2} & 0 \\ C^{EP2} & C^{Ep4} & 0 \\ 0 & 0 & 0 \end{bmatrix} \quad (19)$$

If tensile stress is observed in the interface, both the shear and normal stresses are released. Also, the stiffness normal to the interface and the shear stiffness are assumed to be equal to zero [8]. So, the constitutive matrix in the separation mode can be found as:

$$\left[C^{E}\right] = \begin{bmatrix} C^{E1} & 0 & 0 \\ 0 & 0 & 0 \\ 0 & 0 & 0 \end{bmatrix} \quad (20)$$

Here, the x direction is assumed to be parallel to the interface of soil and structure and the y direction is normal to this interface.

The finite element formulation of the interface element is based on the constitutive matrices presented in Equations 3, 19 and 20, in the stick, slip and separation modes, respectively.

The aspect ratio of the interface elements has been chosen to be equal to 0.025. The large side of the elements are parallel to the wall in the vertical direction. It should be noted that this ratio has been recommended to be between 0.01 and 0.1 [11].

The damping coefficients of the far field vertical boundaries are calculated, for local transmitting boundaries, as [12]:

$$C_H = \rho V_S \quad (21)$$

$$C_V = \rho V_P \quad (22)$$

Here, ρ is the special mass density of the soil medium and V_s and V_p are, respectively, the shear and body wave velocities. Also, C_H and C_V are the horizontal and vertical damping coefficients, respectively.

Damping in the soil and structure has been modeled by Rayleigh method[8]. In this technique, the damping matrix is found using:

$$[C] = a[M] + b[K] \quad (23)$$

In which, [C], [M] and [K], are the damping, mass and stiffness matrices, respectively. The parameters a and b are found by the first two modes through:

$$\frac{a}{2\omega_i} + \frac{b\omega_i}{2} = \xi_i \quad (24)$$

Where, ω_i and ξ_i are, respectively, the circular frequency and damping ratio of mode i. The damping ratio of the soil and the structure are assumed to be equal to 10 and 5 percent of the critical damping, respectively.

It should be noted that the damping of the soil medium is a function of the shear strain. The damping ratio of sand varies between about 6 percent for shear strain equal to 0.0001 to 16 percent for shear strain equal to 0.0008 [13]. In high base accelerations, as in the ones used in this

study, the shear strain reaches 0.0005, and the damping ratio will be about 10 percent of the critical damping.

To incorporate the connectivity of the structural floors to the perimeter walls, the walls and the middle main structure have been constrained at the top and midheight of the walls, so that the wall-structure system experiences equal horizontal displacements at floor levels. This assumption represents the rigidity of floor diaphragms.

The finite element mesh used in the analysis is shown in Figure 4. All of the plane strain elements are 9 noded lagrangian ones each node having two translational degrees of freedom. The interpolation functions in the two local coordinates are parabolic and can be found in classical finite element references [14].

The strain displacement matrix can be calculated as:

$$[B] = [L][N] \tag{25}$$

$$[L] = \begin{bmatrix} \partial/\partial x & 0 \\ 0 & \partial/\partial y \\ \partial/\partial y & \partial/\partial y \end{bmatrix} \tag{26}$$

Here, [B] and [N] are the strain displacement and interpolation matrices, respectively.

The constitutive matrices used in finite element formulation of different parts of the model were presented earlier. The stiffness matrix of the elements are found as:

$$[k] = \int [B]^T [C][B]\, dA \tag{27}$$

In this equation [C] can be elastic or elastoplastic constitutive matrix and A is the area of the element.

The number of the elements in the horizontal direction is constant but in the vertical direction is a function of the height of the wall. The mesh will have 1240 to 1540 nodes, depending on the height of the wall.

The ADINA software has been used to perform the analysis [15]. The interface element has been added to the software. To verify the results of this element, the wall modeled by El-Homoud, et al [16] was analyzed. The top and bottom displacements of the wall under 5 different sinusoidal input motions, types I to V in the reference, were found to have 9 percent difference, on the average, with El Homoud and Whitman results. On the other hand, El Homoud and Whitman have reported 23 percent error, on the average, in computing the displacements of test results using their model [16].

3. OBJECTIVE OF THE ANALYSIS

The analysis is made with the objective to present a dynamic soil thrust diagram for embedded perimeter walls, which can be thought to be rigid compared to the cantilever retaining walls. To achieve this goal, 45 different models have been analyzed changing the parameters.

The natural frequency of the soil is approximated by $V_s/4H$, where V_s which is equal to $(G/\rho)^{0.5}$, is the shear wave velocity in the soil

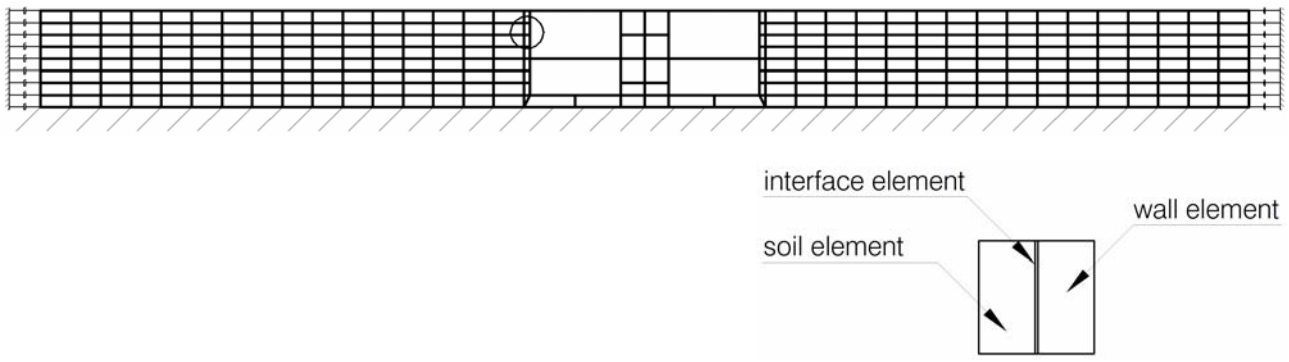

Figure 4. Finite element mesh.

medium. G is the small strain shear modulus of the soil. During the analysis, the density of the soil is set equal to 18 kN/m^3 and the shear modulus is changed to achieve different natural frequencies for the soil medium. The poisson's ratio of the soil material is assumed to be equal to 0.2.

To obtain different natural frequencies for the wall-structure system, consisting of the main central structure and the walls, the density of the structural material in the main middle part is varied. The density of the wall material is set to be equal to 25 kN/m^3 and the modulus of elasticity and Poisson's ratio for the structure and the wall material is assumed to be equal to 20000 mN/m^2 and 0.15, respectively.

As input base acceleration, five types of ricker waves with central frequencies of 1 Hz, 2 Hz, 3 Hz, 4 Hz and 5 Hz, named ricker 1 to ricker 5, having peak accelerations equal to 0.4 g are used [17]. Based on these input base acceleration diagrams, nonlinear time history analysis with 0.01 seconds time intervals will be performed. As a sample, ricker 2 wave is shown in Figure 5. It has been shown that if the dominant frequency of an earthquake is the same as a ricker wave, similar responses will be found [18].

It has been shown by Wu and Finn that the maximum soil trust occurs when the predominant period of the base acceleration is equal to that of the soil medium and to the wall-structure system [2]. The same conclusion was reached by the authors by analyzing an 8 m high wall under the ricker 2 and 4 wavelets, with different ratios of soil medium, structure and input base acceleration frequencies. The frequencies of the soil medium and the structure were varied by changing the soil stiffness and the structure density. Therefore, to find the critical dynamic soil thrust, the frequencies of the soil, the structure and the base acceleration were set to be equal in the present study.

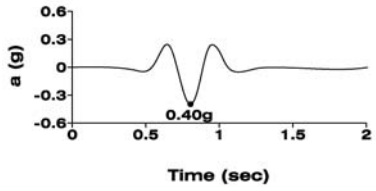

Figure 5. Ricker 2 base acceleration diagram.

It is worth noticing that the maximum values of dynamic pressure on the wall do not occur simultaneously along the height of the wall, but as one may expect the pressure at the top always has the highest value. Thus, the pressure diagrams presented in the next section are drawn at the time when the top pressure is at maximum.

4. RESULTS OF THE ANALYSIS

Before making any discussions on the results obtained by imposing ricker acceleration wavelets, the dynamic pressure induced by ricker 2 and the 1940 ElCentro base motions are compared in Figure 19. Both input accelerations are scaled such that the maximum base acceleration is equal to 0.2 g. In the analysis the height of the wall is assumed to be equal to 8 meters and also the internal friction angle is set equal to 30 degrees. Furthermore, the pressures are found by setting the soil and the structure frequencies equal to the predominant frequency of the input motion. It is noted that the predominant frequency of the El Centro earthquake acceleration time history is 1.85 Hz. Considering Figure 6, it is observed that both excitation motions generate similar results because their frequencies are close to each other.

To show the effect of the soil internal friction angle, the 8 meter high wall is analyzed under

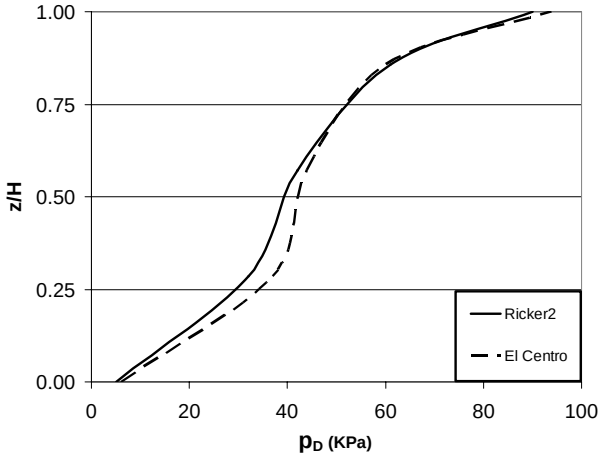

Figure 6. Comparison of ricker 2 and elcentero dynamic pressure.

ricker 2 base accelerations for internal friction angles equal to 30, 40 and 50 degrees. The results are shown in Figure 7. Investigating this figures, it can be found that the pressure is a function of the internal friction angle of the soil and it is decreased by increasing the internal friction angle.

As a measure of the influence of the internal friction angle of the soil, the in situ lateral soil pressure coefficient, K_0, which is equal to 1-sinφ, is employed. Scaling by $K_0A\gamma H$, the seismic pressure on the 8 meter high wall, under ricker base accelerations, and soil internal friction angles equal to 30, 40 and 50 degrees are shown in Figures 8 to 10, respectively.

Next, a 10 meters high wall is analyzed under the same conditions. The seismic pressure diagrams are presented in Figures 11 to 13.
Finally, the same diagrams for a wall 12 meters high are presented in Figures 14 to 16.

5. PROPOSED DYNAMIC PRESSURE DIAGRAM

Based on the data gathered in the previous section, a linear regression analysis is performed and thus a linear diagram for the distribution of the seismic pressure is proposed. This regression is based on the 84th percentile, which is assumed as a suitable level for design purposes [2]. The proposed diagram is a function of the maximum base acceleration with respect to gravity acceleration (A), the height of the wall (H), the density of the soil (γ), and the in situ lateral soil pressure coefficient (K_0). The dynamic pressure distribution, obtained in this form and shown in Figure 17, can be written as:

$$P_D = [3.35\ (z/H) + 0.8]K_0A\gamma H \qquad (28)$$

The proposed diagram is based on the assumption of damping ratios of the structure and the soil being equal to 0.05 and 0.1, respectively. If the damping ratio of the soil is assumed to be equal to 5 percent of the critical damping, an average of about 9 percent increase in the soil thrust is observed. Thus, it is recommended to use a conservative damping modification factor equal to 1.1 for the dynamic pressure if the maximum base

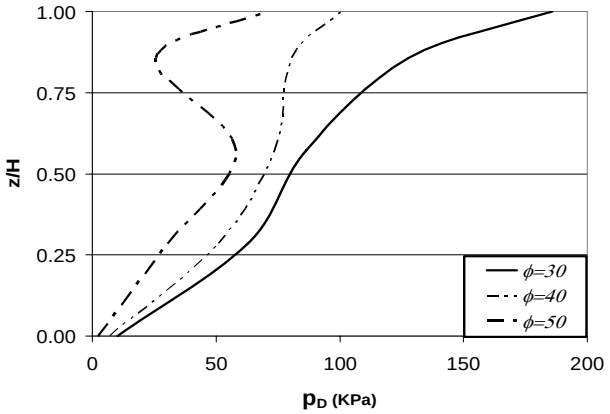

Figure 7. Effect of soil internal friction angle on dynamic pressure.

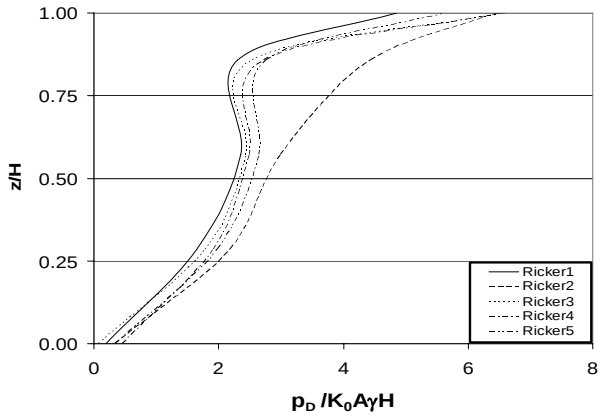

Figure 8. Dynamic pressure diagram on 8 m high wall for φ = 30.

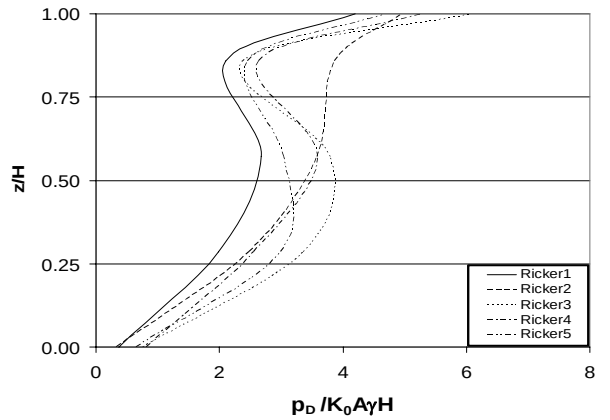

Figure 9. Dynamic pressure diagram on 8 m high wall for φ = 40.

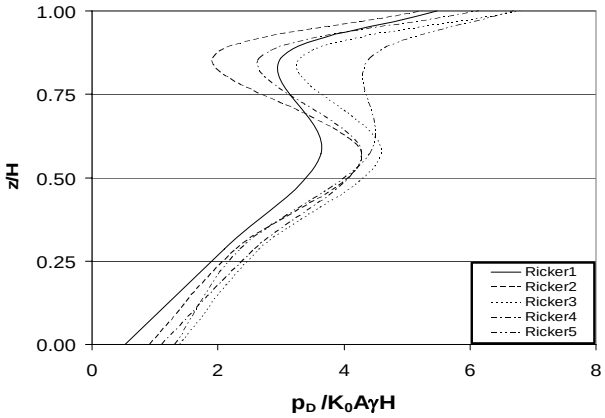

Figure 10. Dynamic pressure diagram on 8 m high wall for φ = 50.

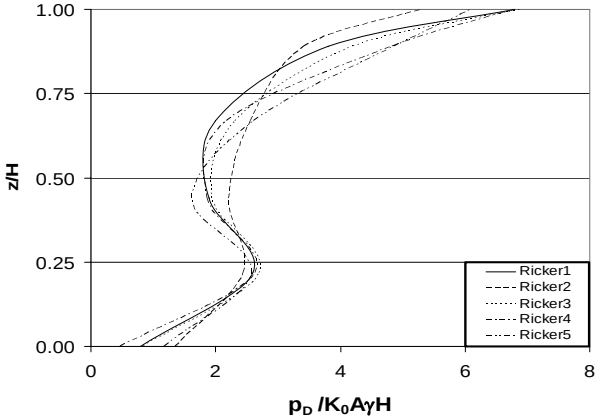

Figure 13. Dynamic pressure diagram on 10 m high wall for φ = 50.

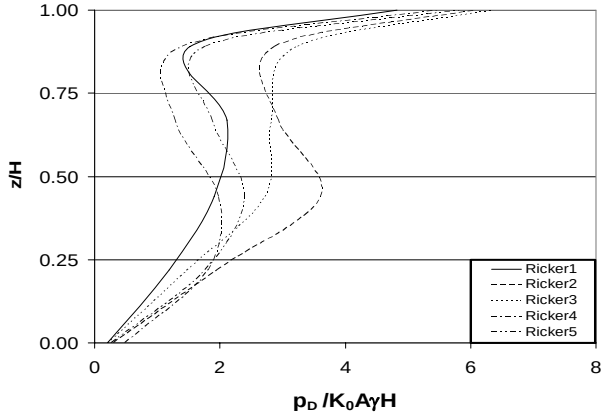

Figure 11. Dynamic pressure diagram on 10 m high wall for φ = 30.

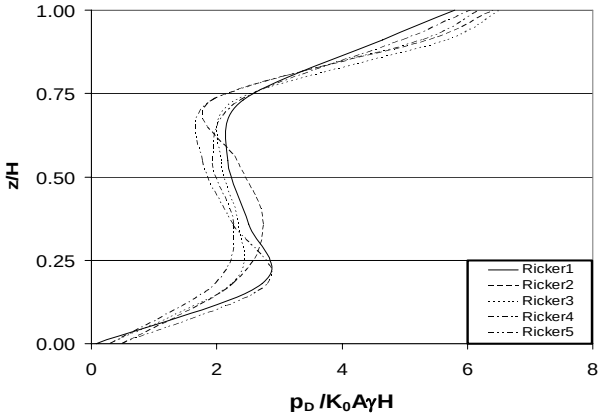

Figure 14. Dynamic pressure diagram on 12 m high wall for φ = 30.

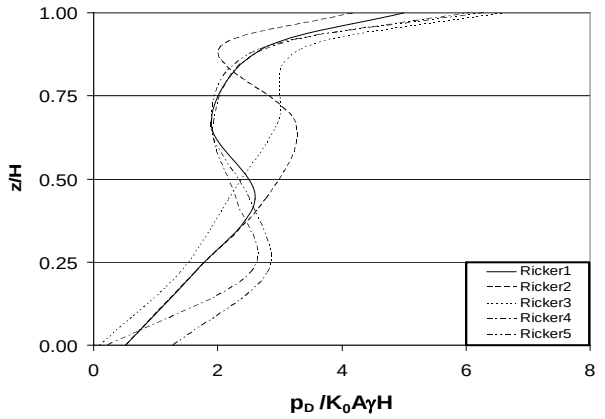

Figure 12. Dynamic pressure diagram on 10 m high wall for φ = 40.

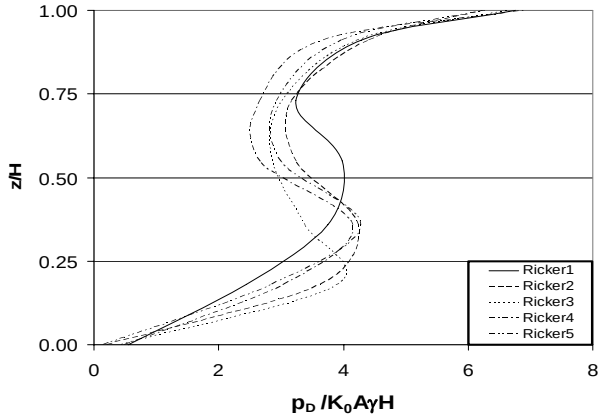

Figure 15. Dynamic pressure diagram on 12 m high wall for φ = 40.

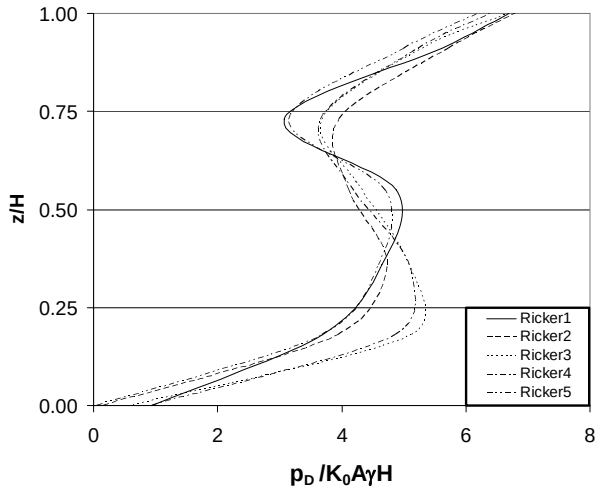

Figure 16. Dynamic pressure diagram on 12 m high wall for φ = 50.

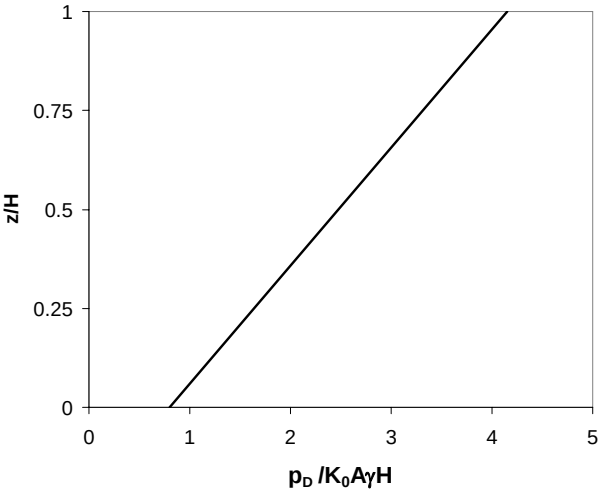

Figure 17. Proposed seismic soil pressure.

acceleration is lower than 0.25 g, because the soil will experience lower shear strains.

Furthermore, the effect of the Poisson's ratio of the soil was investigated. It was found that the modification factor recommended by Veletsos and Younan can be used [19]. If the Poisson's ratio of the soil material is shown by υ, this factor is defined by:

$$\psi(\nu) = 2/[(1-\upsilon)(2-\upsilon)]^{0.5} \quad (29)$$

If the poisson's ratio of the soil is not equal to 0.2, then the modification factor will be equal to $\psi(\nu)/\psi(0.2)$.

The GRG and ASCE diagrams are compared with the proposed diagram presented in the previous section. Figures 18 through 20 show the results of comparison for angles of internal friction equal to 30, 40 and 50 degrees, respectively. It is observed that GRG and ASCE standards that neglect the effect of internal friction angle can be non-conservative for lower internal friction angles.

For friction angle equal to 30 degrees, the total dynamic force on the wall in this study is about 38 percent higher than Wood and 24 percent higher than GRG one. On the other hand, if internal friction angle is equal to 40 degrees, the total force found in this study will be about 1 and 11 percent lower than Wood and GRG solutions. Also, for internal friction angle equal to 50 degrees, the total lateral force will be about 36 percent lower than Wood and 42 percent lower than GRG forces. Furthermore, the height of center of pressure will be equal to 0.613 H which is between Wood and GRG solutions. It is noted that Wood and GRG solutions gives the height of application of seismic thrust equal to 0.63 H and 0.58 H, respectively.

Also, the total dynamic soil thrust in the formula proposed in this study will match the Wu and Finn diagrams for the uniform, linear and parabolic variation of G, if the internal friction angle is set equal to 27, 37 and 33 degrees, respectively. It should be noted that in the Wu and Finn diagrams the height of the resultant seismic thrust varies between 0.5 H to 0.64 H.

6. EXAMPLES

As an example a frame bridge, shown in Figure 21, consisting of a slab deck with depth of 800 mm and abutment walls with width of 600 mm is analyzed. The deck and the abutment wall have continuous connection that makes a rigid frame.

The parameters φ, A and γ are assumed to be equal to 35, 0.3 and 20 kN/m^3, respectively. The modulus of elasticity and poisson's ratio of the structural material are assumed to be equal to 25000 Mpa and 0.15, respectively.

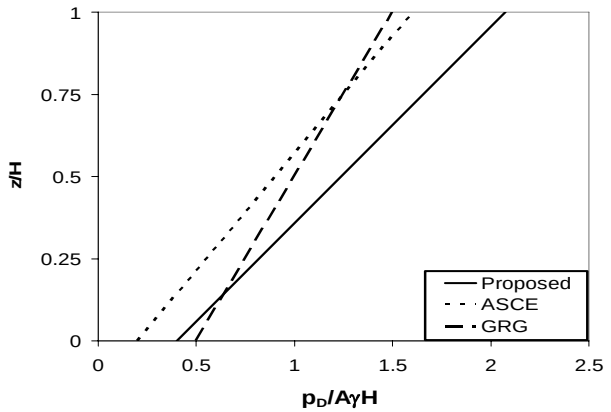

Figure 18. Comparison of the proposed diagram with ASCE and GRG diagrams for φ = 30.

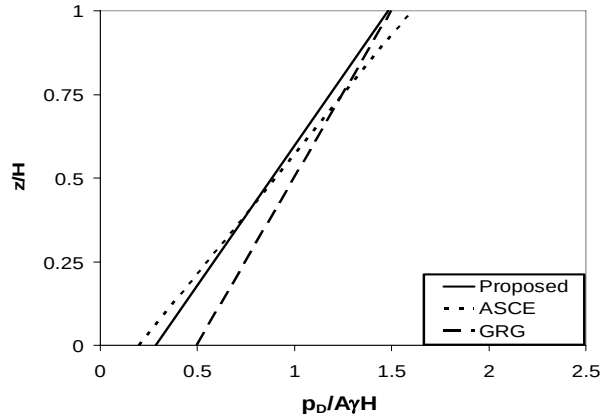

Figure 19. Comparison of the proposed diagram with ASCE and GRG diagrams for φ = 40.

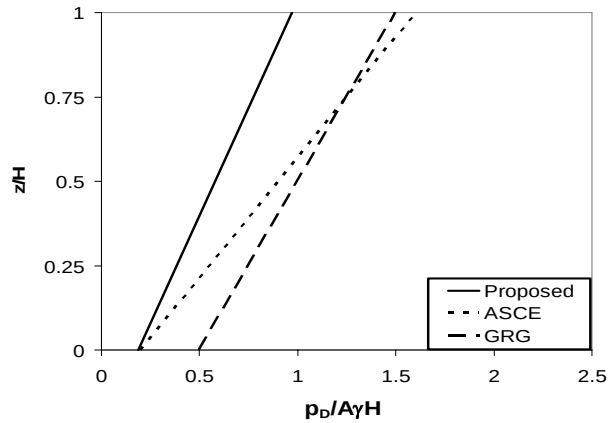

Figure 20. Comparison of the proposed diagram with ASCE and GRG diagrams for φ = 50.

The proposed pressure diagram of this study along with the ASCE and GRG pressure diagrams are employed in the analysis. The results show that the moment in the deck slab using the proposed diagram is 15.3 and 8.8 percent higher than the ASCE and GRG diagrams, respectively. The maximum moment in the wall shows 18.7 and 3.3 percent increase for the proposed method with respect to the ASCE and GRG responses, respectively. On the other hand, the base shear in the wall, for the proposed thrust diagram is 22.5 percent higher than the ASCE but 1.8 percent lower than the GRG method.

As another example, a 6 story, 2 bay building frame as shown in Figure 22 is analyzed under soil dynamic pressure on the left 2 bottom stories. The soil internal friction angle is assumed to be equal to 30 degrees and the soil density equal to 18KN/m^3. Also, the maximum base acceleration is assumed to be equal to 0.3 g.

The beams have 300 mm width and 500 mm depth. The columns width and depth are 500 mm. The modulus of elasticity and poisson's ratio of the structural material are assumed to be equal to 25000 Mpa and 0.15, respectively.

The Top story lateral displacement is found to have 33.6 and 31.9 percent increase in the proposed method with respect to the ASCE and GRG codes, respectively. Also, the base shear shows 32.5 and 23.5 percent increase in the analysis using the proposed dynamic pressure diagram with respect to the ASCE and GRG methods, respectively. This example shows clearly that for low soil internal friction angles, the ASCE and GRG methods can lead to nonconservative results.

7. CONCLUSION

To find the dynamic soil pressure on typical buried perimeter retaining walls of a structure, nonlinear soil model in addition to modeling the interface between soil and structure has been used. Previous investigations have been limited to simple models of the problem, such as assuming a hinged support at the top level of the wall. Also, the soil behavior has been assumed to be elastic.

In the models used in the codes the effects of

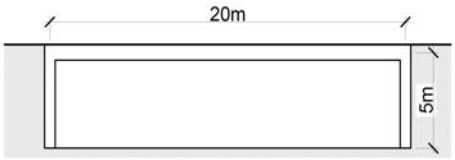

Figure 21. Frame bridge.

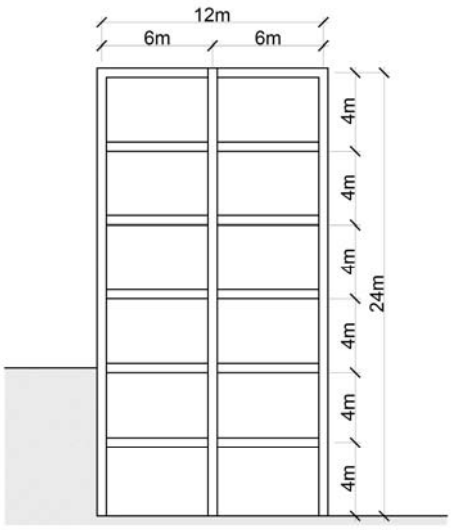

Figure 22. Building frame.

the internal friction angle of the soil is neglected, although it has an important influence on the magnitude of dynamic pressure and also on the height of the center of the dynamic thrust. In this paper, a linear seismic soil thrust distribution against rigid walls, which is as function of the internal friction angle, has been proposed.

8. NOTATION

A	Maximum Ground Acceleration Coefficient
C_H	Horizontal Damping Coefficient
C_V	Vertical Damping Coefficient
E	Elasticity Modulus
G	Shear Modulus
H	Height of the Wall
I_1	First Stress Invariant
J_2	Second Deviatory Stress Invariant
K_0	In Situ Lateral Soil Pressure Coefficient
p_D	Dynamic Soil Pressure
V_s	Shear Wave Velocity
V_p	Body Wave Velocity
[C]	Damping Matrix
$[C^E]$	Elastic Constitutive Matrix
$[C^{EP}]$	Elastoplastic Constitutive Matrix
[K]	Stiffness Matrix
[N]	Interpolation Matrix
γ	Soil Density
φ	Internal Friction Angle of the Soil
ρ	Special Mass Density
ξ	Damping Ratio
ω	Circular Frequency
υ	Poisson's Ratio

9. REFERENCES

1. Wood, J. H., "Earthquake Induced Soil Pressures on Structures", Doctoral Dissertation, EERL, California Institute of Technology, Pasadena, CA, (1973), 73-05.
2. Wu, G. and Finn, W. D. L., "Seismic Lateral Pressures for Design of Rigid Walls", ***Canadian Geotechnical Journal***, Vol. 36, (1999), 509-522.
3. Ostadan, F. and White, W. H., "Lateral Seismic Soil Pressure, An Updated Approach", US Japan SSI Workshop, Menlo Park, California, U.S.A., (1998).
4. Younan, A. H. and Veletsos, A. S., "Dynamic Response of Flexible Retaining Walls", ***Earthquake Engineering and Structural Dynamics***, Vol. 29, (2000), 1815-1844.
5. ASCE 4.86, "Seismic Analysis of Safety Related Nuclear Structures", American Society of Civil Engineers, Washington, U.S.A., (1986).
6. Regulatory Guide E39/93 for the Seismic Analysis of Bridges, Ministry of Public Works, Bulletin of Greek Technical Chamber, No. 2040, Athens, (1998).
7. Potts, D. M. and Zdravkovic, L., "Finite Element Analysis in Geotechnical Engineering", Theory, Thomas Telford, London, U.K., (1999).
8. Bathe, K. J., "Finite Element Procedures", Prentice Hall, Englewood Cliffs, New Jersey, U.S.A., (1996).
9. Ze, Y. Z. and Hong, Z., "A Study of Deformation in the Interface Between Soil and Concrete", ***Computers and Geotechnics***, Vol. 17, (1995), 75-92.
10. Zaman, M., Chandrakant, S., Desai, M. and Drumm, E. C., "Interface Model for Dynamic Soil Structure Interaction", ***Journal of Geotechnical Engineering***, Vol. 110, No. 9, (1984), 1257-1273.
11. Desai, C. S., Zaman, M. M., Lightner, G. and Siriwardane, H. J., "Thin Layer Element for Interfaces and Joints", ***International Journal of Numerical and***

Analytical Methods in Geomechanics, No. 8, (1984), 19-43.
12. Kausel, E., "Local Transmitting Boundaries", ***Journal of Engineering Mechanics, ASCE***, Vol. 114, (1988), 1011-1027.
13. Choi, J. S., Yun, C. B. and Kim, J. M, "Earthquake Response Analysis of the Hualien Soil Structure Interaction System based on Updated Soil Properties using Forced Vibration Test Data", ***Earthquake Engineering and Structural Dynamics***, No. 30, (2001), 1-26.
14. Kardestuncer, H., "Finite Element Handbook", McGrawHill, New York, U.S.A., (1987).
15. Bathe, K. J., "ADINA User's Manual", Watertown, ADINA Engineering INC, Watertown, MA, (1984).
16. Al-Hamoud, A. S. and Whitman, R. V., "Seismic Analysis and Design of Rigid Bridge Abutments Considering Rotation and Sliding Incorporating Nonlinear Soil Behavior", ***Soil Dynamics and Earthquake Engineering***, No. 18, (1999), 247-277.
17. Ricker, N., "The Form and Laws of Propagation of Seismic Wavelets", ***Geophysics***, (1973), 18-40.
18. Gazetas, G., Psarroupoulos P. N., Anastasopoulos, I. and Gerolymos, N., "Seismic Behavior of Flexible Retaining Systems Subjected to Short Duration Moderately Strong Excitation", ***Soil Dynamics and Earthquake Engineering***, Vol.24, (2004), 537-550.
19. Veletsos, A. and Younan, A. H., "Dynamic Soil Pressure on Rigid Vertical Walls", ***Soil Dynamics and Earthquake Engineering***, Vol. 23, (1994), 275-301.